2017

Capillary-Induced Ge Uniformly Distributed in N-Doped Carbon Nanotubes with Enhanced Li-Storage Performance

Haipeng Guo
University of Wollongong, hg476@uowmail.edu.au

Boyang Ruan
University of Wollongong, br970@uowmail.edu.au

Lili Liu
University of Wollongong, ll422@uowmail.edu.au

Lei Zhang
University of Wollongong, lz755@uowmail.edu.au

Zhanliang Tao
University of Wollongong, *Nankai University*, ztao@uow.edu.au

See next page for additional authors

Publication Details

Guo, H., Ruan, B., Liu, L., Zhang, L., Tao, Z., Chou, S., Wang, J. & Liu, H. (2017). Capillary-Induced Ge Uniformly Distributed in N-Doped Carbon Nanotubes with Enhanced Li-Storage Performance. Small, 13 (28), 1700920-1-1700920-7.

Capillary-Induced Ge Uniformly Distributed in N-Doped Carbon Nanotubes with Enhanced Li-Storage Performance

Abstract
Germanium (Ge) is a prospective anode material for lithium-ion batteries, as it possesses large theoretical capacity, outstanding lithium-ion diffusivity, and excellent electrical conductivity. Ge suffers from drastic capacity decay and poor rate performance, however, owing to its low electrical conductivity and huge volume expansion during cycling processes. Herein, a novel strategy has been developed to synthesize a Ge at N-doped carbon nanotubes (Ge at N-CNTs) composite with Ge nanoparticles uniformly distributed in the N-CNTs by using capillary action. This unique structure could effectively buffer large volume expansion. When evaluated as an anode material, the Ge at N-CNTs demonstrate enhanced cycling stability and excellent rate capabilities.

Keywords
enhanced, nanotubes, carbon, n-doped, distributed, uniformly, ge, performance, li-storage, capillary-induced

Disciplines
Engineering | Physical Sciences and Mathematics

Publication Details
Guo, H., Ruan, B., Liu, L., Zhang, L., Tao, Z., Chou, S., Wang, J. & Liu, H. (2017). Capillary-Induced Ge Uniformly Distributed in N-Doped Carbon Nanotubes with Enhanced Li-Storage Performance. Small, 13 (28), 1700920-1-1700920-7.

Authors
Haipeng Guo, Boyang Ruan, Lili Liu, Lei Zhang, Zhanliang Tao, Shulei Chou, Jiazhao Wang, and Hua-Kun Liu

ADVANCED SCIENCE NEWS
www.advancedsciencenews.com

Capillary-Induced Ge Uniformly Distributed in N-Doped Carbon Nanotubes with Enhanced Li-Storage Performance

Haipeng Guo, Boyang Ruan, Lili Liu, Lei Zhang, Zhanliang Tao, Shulei Chou, Jiazhao Wang, and Huakun Liu**

Germanium (Ge) is a prospective anode material for lithium-ion batteries, as it possesses large theoretical capacity, outstanding lithium-ion diffusivity, and excellent electrical conductivity. Ge suffers from drastic capacity decay and poor rate performance, however, owing to its low electrical conductivity and huge volume expansion during cycling processes. Herein, a novel strategy has been developed to synthesize a Ge@N-doped carbon nanotubes (Ge@N-CNTs) composite with Ge nanoparticles uniformly distributed in the N-CNTs by using capillary action. This unique structure could effectively buffer large volume expansion. When evaluated as an anode material, the Ge@N-CNTs demonstrate enhanced cycling stability and excellent rate capabilities.

Lithium-ion batteries (LIBs), as the most advanced energy storage device, have been widely applied in electrical vehicles, portable electronics, and smart grids.[1,2] The commercialized graphite anodes, however, cannot satisfy the demand for high-energy, next-generation batteries because of the low theoretical specific capacity (372 mAh g^{-1}) of graphite.[3] Therefore, anode materials with high capacity have been introduced, such as Si, Ge, and Sn.[4,5] Among these, germanium has attracted considerable attention as a superior anode material owing to its excellent electrical conductivity, outstanding lithium-ion diffusivity, and large theoretical capacity.[6–9] Similar to other anode materials (like silicon and tin), however, Ge also suffers from drastic capacity decay and poor rate performance owing to the severe volume changes (about 300%) during repeated charge/discharge processes.[10] One approach to improving the electrochemical performance is to use nanosized materials, especially 1D nanotubes or nanowire structures, due to their short lithium-ion diffusion lengths and excellent electrical conductivities.[11–17] Many strategies have been developed to synthesize 1D structured materials, such as the hydrothermal,[15,16] chemical-vapor deposition,[18–22] electrospinning,[23] and chemical polymerization[24] methods. Another method is to use a carbon matrix, which could accommodate volume changes, enhance electrical conductivity of the electrode, and serve as an active material for lithium storage.[25–28] In particular, nanoparticles encapsulated in carbon nanotubes represent the most desirable structure, which could not only benefit from the advantages of 1D structure, but also provide void spaces to buffer the volume changes of active materials.[29–32] For example, Chu and co-workers prepared peapod-like Ge/CN_x with Ge incorporated in a CN_x layers by using a chemical polymerization method to coat a polypyrrole layer on the surfaces of GeO_2 nanowires.[29] Yu and co-workers synthesized carbon-nanofiber-encapsulated Ge nanoparticles through the electrospinning method.[32] The active material nanoparticles were not very uniformly distributed within the carbon nanotubes, however, which may mean that the void spaces cannot

H. Guo, B. Ruan, L. Liu, L. Zhang, Prof. Z. Tao,
Dr. S. Chou, Prof. J. Wang, Prof. H. Liu
Institute for Superconducting and Electronic Materials
University of Wollongong
Squires Way, North Wollongong, NSW 2500, Australia
E-mail: jiazhao@uow.edu.au; hua@uow.edu.au
Prof. Z. Tao
Key Laboratory of Advanced Energy Materials
Chemistry (Ministry of Education)
College of Chemistry
Nankai University
Tianjin 300071, China

DOI: 10.1002/smll.201700920

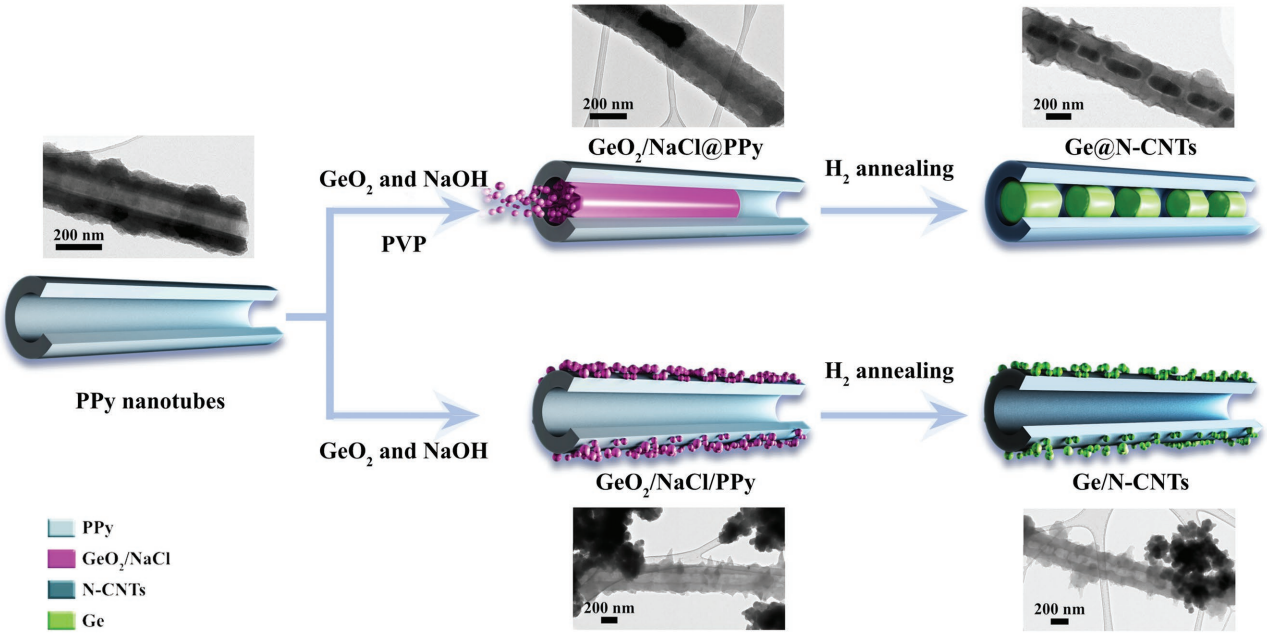

Figure 1. Illustration of the synthesis processes for the Ge@N-CNTs and Ge/N-CNTs composites.

be fully utilized to accommodate volume changes. Therefore, it is extremely attractive to design a novel strategy to synthesize 1D structured materials with uniformly distributed active materials.

Capillary action is a facile strategy to synthesize novel 1D structured materials through filling the hollow cavities of nanotubes with the chosen materials.[33] Numerous efforts have been devoted to drawing different foreign materials in the liquid or molten phase into the hollow inner cavities by using capillary action to synthesize 1D structured materials.[34–39] The surface tension of the foreign materials, however, is the most important parameter for successful filling, which should be less than 200 mN m^{-1}.[40] Hence, only materials with low surface tension could be introduced into the hollow cavities by using capillary action. Therefore, it is still a big challenge to introduce high surface tension materials into the inner hollow cavities to fabricate 1D structured materials, which are expected to provide breathtaking opportunities for practical applications and fundamental research.

Herein, we present a feasible strategy to synthesize core–shell GeO_2/NaCl@polypyrrole nanotubes by utilizing capillary action, which could be further transformed into a 1D Ge@N-doped carbon nanotubes (Ge@N-CNTs) composite, with Ge nanoparticles uniformly distributed in the N-CNTs. The successful fabrication of Ge nanoparticles uniformly encapsulated in N-CNTs lies in two key aspects. First, as a high surface tension material, GeO_2 (250 mN m^{-1}) could not be directly introduced into the hollow cavities in the molten phase by using capillary action.[41] Even after it is dissolved in NaOH solution to form a liquid phase, the surface tension of the solution is still larger than the cut-off value, which also cannot be introduced into the hollow cavities by using capillary action. The surface tension could be decreased, however, through adding poly(vinylpyrrolidone) (PVP), and then the solution could be induced into the robust PPy nanotubes to form the core–shell GeO_2/NaCl@polypyrrole (PPy) nanotubes composite by utilizing capillary action. Second, through reducing GeO_2 to Ge and removing NaCl with a further annealing and centrifuging treatment, a composite of Ge nanoparticles uniformly distributed in the N-CNTs could be obtained. The uniformly distributed Ge nanoparticles could effectively utilize the void spaces provided by the unique 1D structure during cycling, which could preserve the original structure of the Ge@N-CNTs and achieve prolonged cycling stability. When investigated its lithium storage performance, the Ge@N-CNTs demonstrated enhanced cycling stability and excellent rate capacity.

The synthesis process to fabricate the Ge@N-CNTs and Ge/N-CNTs composites is illustrated in **Figure 1**. First, uniform PPy nanotubes with a hollow inner cavity and open tips, which are favorable for capillary action, are synthesized through the polymerization method in a relatively large quantity. Second, the PPy nanotubes are mixed with a GeO_2 and NaOH aqueous solution, followed by adjusting the pH of the solution to 7 with diluted HCl. Then, PVP is added into the solution, which can decrease the surface tension and thus increase the effect of capillary action to fill the inner hollow cavities with GeO_2/NaCl in an aqueous solution.[42] Therefore, by utilizing capillary action, a core–shell GeO_2/NaCl@PPy nanotubes composite is formed through inducing GeO_2/NaCl into the inner hollow cavities after drying at 60 °C. Finally, the unique 1D structured Ge@N-CNTs composite with Ge nanoparticles uniformly encapsulated in N-CNTs is obtained through a carbonization and annealing process in H_2 atmosphere, followed by the removal of NaCl by centrifuging. As shown in the transmission electron microscope (TEM) images (Figure 1) and the scanning electron microscope (SEM) images (Figure S1, Supporting Information), the PPy nanotubes with an inner cavity diameter of about 100 nm and open tips can be directly used for capillary action without any further treatment. The successful synthesis

of core–shell GeO_2/NaCl@PPy nanotubes could be further confirmed by elemental mapping images (**Figure 2**), which reveal that GeO_2 and NaCl are completely filled into the hollow inner cavity and uniformly distributed along the axial direction of a nanotube. The GeO_2/NaCl could not be induced into the hollow cavities of PPy nanotubes, however, without adding PVP. This was because the surface tension of GeO_2/NaCl solution is too high to draw GeO_2/NaCl into the inner hollow cavities. All of the GeO_2/NaCl nanoparticles are dispersed on the outside of the PPy nanotubes instead of filling the hollow cavities. Therefore, Ge/N-CNTs with Ge nanoparticles aggregated on the outside of the N-CNTs could be obtained after further annealing and centrifugal treatment (Figure 1 and Figure S2, Supporting Information). This implies that the PVP could increase the effect of capillary action through decreasing the surface tension. Moreover, the distribution of the nanoparticles in the composite could be easily tuned by adjusting the surface tension. During the heating process, the N-CNTs content was totally burned out, and the Ge was oxidized into GeO_2 with increasing temperature. Therefore, based on the weight of GeO_2, the content of Ge can be calculated. By using this method, the Ge contents are determined to be 70.5 and 72.5 wt% in the Ge/N-CNTs and Ge@N-CNTs, respectively, according to the thermogravimetric analysis data (Figure S3, Supporting Information).

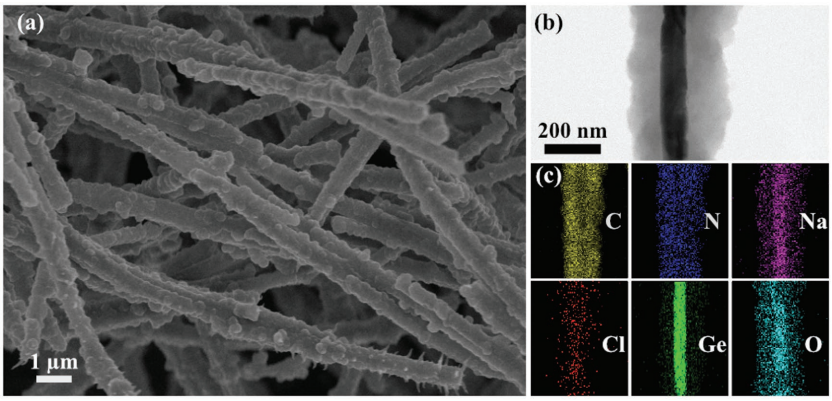

Figure 2. a) SEM image, b) TEM image, and c) corresponding elemental mapping images of core–shell GeO_2/NaCl@PPy nanotubes.

The X-ray diffraction (XRD) patterns are manifested in **Figure 3**a. The XRD peaks of the Ge@N-CNTs and

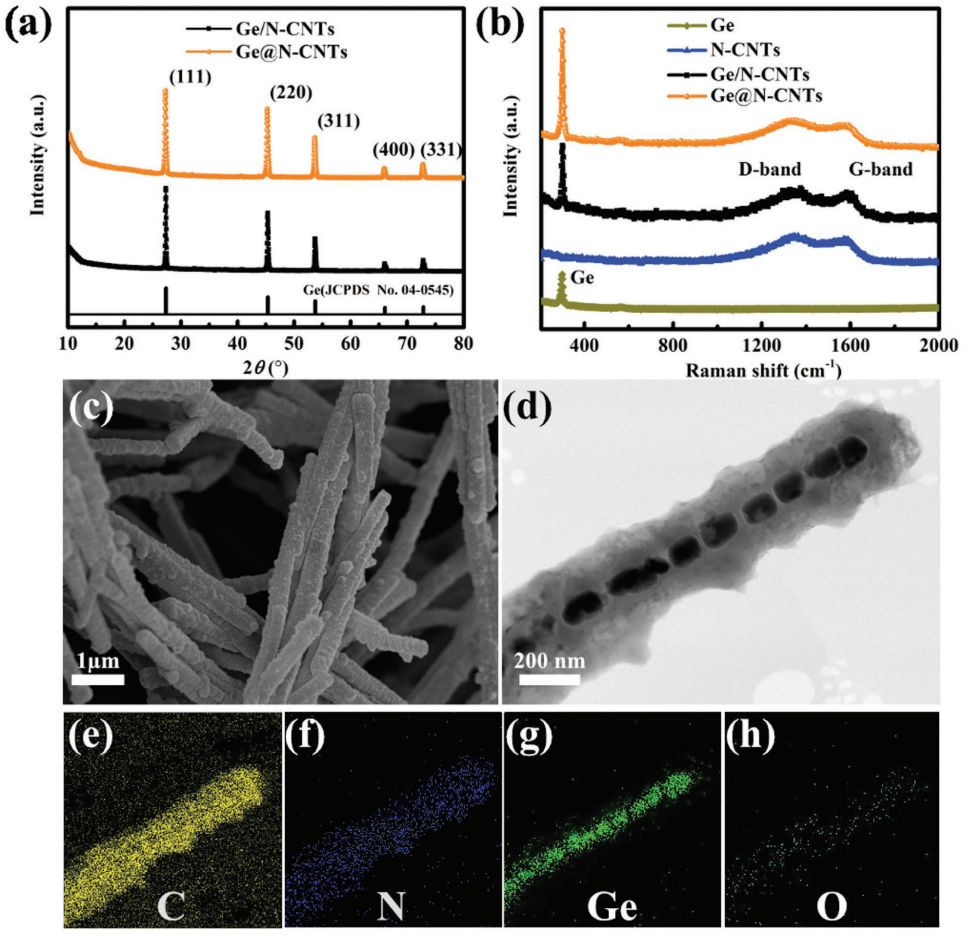

Figure 3. a) XRD patterns of Ge/N-CNTs and Ge@N-CNTs. b) Raman spectra of Ge, N-CNTs, Ge/N-CNTs, and Ge@N-CNTs. c) SEM and d) bright-field TEM images of Ge@N-CNTs. Elemental mapping images of e) C, f) N, g) Ge, and h) O of an individual Ge@N-CNTs nanotubes.

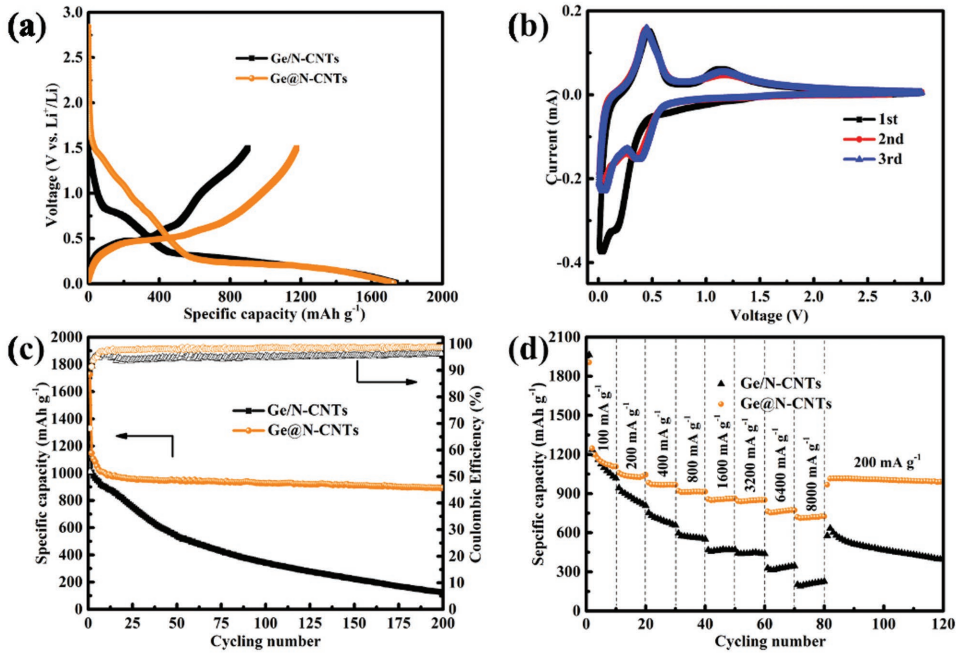

Figure 4. a) First cycle discharge/charge voltage curves of Ge/N-CNTs and Ge@N-CNTs composites cycled at a current density of 100 mA g^{-1} between 0.01 and 1.5 V. b) Cyclic voltammetry profiles of Ge@N-CNTs at a scan rate of 0.1 mV s^{-1} for the first three cycles. c) Cycling stability of the Ge/N-CNTs and Ge@N-CNTs composites at a constant current density of 100 mA g^{-1} between 0.01 and 1.5 V. d) Rate capabilities of Ge/N-CNTs and Ge@N-CNTs at different current densities.

Ge/N-CNTs could be assigned to the cubic Ge (JCPDS No. 04-0545) without any impurities, demonstrating that the GeO_2 has been successfully reduced to Ge and that the NaCl has been fully removed. In addition, no obvious carbon diffraction peak can be detected because of the amorphous nature of the N-CNTs. The Raman spectra are shown in Figure 3b. For pure Ge, the peak centered at 300 cm^{-1} could be assigned to metallic Ge. As for the pure N-CNTs, peaks located at 1350 and 1580 cm^{-1} can be indexed to the D and G bands, respectively. Therefore, three peaks appeared at 300, 1350, and 1580 cm^{-1} for the Ge@N-CNTs and Ge/N-CNTs, which can be attributed to metallic Ge, the D and G bands of N-CNTs, respectively. It is worth mentioning that $FeCl_3$ could be easily washed away after centrifugal treatment with ethanol and deionized water during the synthesis process of PPy nanotubes. In addition, there is no peak of residual Fe in the XRD patterns and Raman spectra, indicating that there is no Fe in the final product. As can be observed from the SEM image (Figure 3c), a large quantity of Ge@N-CNTs composite generally inherits the uniform tubular structure and diameter of the core–shell GeO_2/NaCl@PPy nanotubes. The TEM image (Figure 3d and Figure S4, Supporting Information) further shows the details of the unique Ge@N-CNTs composite. The dark inner Ge cores are homogeneously encapsulated by the N-CNTs shells, and there are some void spaces not only between the individual Ge nanoparticles, but also between the Ge core and the N-CNTs shells. These uniformly distributed Ge nanoparticles could effectively use these void spaces to accommodate a large volume expansion during the cycling processes, thus preventing agglomeration of the electrode materials. It is notable that these void spaces are generated not only from the reduction treatment of GeO_2 in H_2 gas, but also from the removal of NaCl after centrifuge treatment. The elemental mapping results for C, N, and Ge further demonstrate that the Ge nanoparticles are uniformly distributed along the axial direction of the tube (Figure 3e–g). Moreover, the N doping in the CNTs could improve the electrical conductivity, which additionally contributes to the enhanced electrochemical performance. In addition, as shown in Figure 3h, the element mapping for oxygen is negligible, indicating that the GeO_2 has been completely reduced to Ge during the annealing treatment. This maybe because the PPy nanotubes have open ends, which could allow the hydrogen gas flow into the cavities and reduce the GeO_2. All of these data demonstrate the successful fabrication of this unique Ge@N-CNTs structure with Ge nanoparticles uniformly encapsulated in the N-CNTs.

To demonstrate the structural advantages of the Ge@N-CNTs, the electrochemical performances of both the Ge@N-CNTs and the Ge/N-CNTs composites were investigated. The specific capacity was calculated using both N-CNTs and Ge composite. **Figure 4**a presents the first cycle discharge/charge curves of the Ge@N-CNTs and Ge/N-CNTs composites at a current density of 100 mA g^{-1} in the potential range of 0.01–1.5 V versus Li/Li^+. The Ge/N-CNTs exhibit initial discharge and charge capacities of 1737 and 900 mAh g^{-1}, respectively, with a Coulombic efficiency of 52%. On the other hand, the Ge@N-CNTs composite shows a higher initial Coulombic efficiency of 68%, and its initial discharge and charge capacities are 1725 and 1176 mAh g^{-1}, respectively. The lithium storage mechanism of the Ge@N-CNTs was investigated by using cyclic voltammetry (CV), as shown in Figure 4b. There is a small reduction peak located at 0.16 V in the first cycle, which could be attributed to the formation

of Li–Ge phase.[43–46] This peak disappears, however, after the first cycle, and new peak appears at 0.36 V, suggesting the phase transition from lithiated Li_xGe to amorphous Ge.[47] In the case of Ge/N-CNTs, there is an obvious reduction peak centered at 1.3 V in the first cycle, which could be assigned to the formation of a solid electrolyte interphase (SEI) film between the Ge nanoparticles and the electrolyte (Figure S5, Supporting Information). Figure 4c presents the cycling stability of the Ge@N-CNTs and Ge/N-CNTs composites at a constant current density of 100 mA g^{-1} in the potential range of 0.01–1.5 V. Clearly, the Ge@N-CNTs presents an enhanced cycling stability and higher reversible capacity compared to the Ge/N-CNTs. Specifically, the Ge@N-CNTs composite still delivers a high discharge capacity of 892 mAh g^{-1} beyond 200 cycles. Moreover, it demonstrates better Coulombic efficiency compared to the Ge/N-CNTs, showing the better reversibility of the Ge@N-CNTs (Figure 4c and Figure S6, Supporting Information). The rapid capacity fading is due to the huge volume changes during the cycling process, which would not only lead to the pulverization and loss of active material, but also the continuous regeneration of the SEI film. As for the Ge@N-CNTs, the enhanced cycling stability demonstrates the advantages of the unique 1D structure, which could preserve the stable SEI films by accommodating the large volume expansion. The rate capabilities of the Ge@N-CNTs and Ge/N-CNTs composites were also investigated at various current densities. The Ge@N-CNTs shows considerably improved rate performance when compared with the Ge/N-CNTs at all high current densities (Figure 4d). The specific capacities of the Ge@N-CNTs composite at the current densities of 3200 and 6400 mA g^{-1} were still 850 and 770 mAh g^{-1}, respectively. The Ge@N-CNTs still deliver a reversible capacity of 725 mAh g^{-1}, even at the high current rate of 8000 mA g^{-1}, whereas the Ge/N-CNTs only exhibit an average capacity of 220 mAh g^{-1} at the current rate of 8000 mA g^{-1}. In addition, the Ge@N-CNTs composite shows very good cycling stability at high current density. As shown in Figure S7 (Supporting Information), Ge@N-CNTs still deliver a reversible capacity of 715 mAh g^{-1} over 180 cycles at the current density of 8000 mA g^{-1}. The enhanced electrochemical performance of the Ge@N-CNTs composite could be attributed to the unique Ge nanoparticles encapsulated in the N-CNTs shells. Specifically, the Ge nanoparticles could facilitate Li^+ ion transport through reducing the diffusion distance. Furthermore, the void spaces and the N-CNTs could effectively suppress the huge volume expansion during cycling processes. In addition, the interconnected network of the N-CNTs could afford good electrical conductivity of the electrode and prevent electrical isolation after prolonged cycling. Therefore, when investigated as anode material, the Ge@N-CNTs composite manifests high specific capacity, enhanced cycling stability, and excellent rate capacity. The structural stability of the Ge@N-CNTs and Ge/N-CNTs was also investigated with ex situ TEM after alloying and dealloying. As can be seen from the TEM image (Figure S6a, Supporting Information), the 1D structure of the Ge@N-CNTs is well preserved after full alloying. Li_xGe completely fills the inner hollow cavity, and the diameter of the nanotube increases from 300 nm to about 500 nm, indicating that the void spaces and N-CNTs could effectively accommodate the volume expansion. Moreover, the structure recovered well after the dealloying process, and the Ge nanoparticles became porous after the extraction of Li during the recharge process (Figure S6b, Supporting Information), which is consistent with previous reports.[48,49] For the Ge/N-CNTs composite, on the other hand, the bare Ge nanoparticles aggregated together after full lithiation, with the diameter of the N-CNTs slightly increased from 300 to 330 nm (Figure S6c, Supporting Information). Furthermore, after dealloying, the size of the Ge particles became significantly smaller after the extraction of Li (Figure S6d, Supporting Information), which would lead to the continuous regeneration of SEI film in the following cycles. As shown in Figure S9 (Supporting Information), even after 200 cycles, the unique 1D structure of the Ge@N-CNTs could be well preserved. These results imply enhanced structural stability of the unique 1D structure, with Ge nanoparticles uniformly distributed in the N-CNTs during cycling, which results in the enhanced electrochemical performance of the Ge@N-CNTs.

In conclusion, we have presented a novel strategy to fabricate Ge@N-CNTs composite with Ge nanoparticles uniformly encapsulated in N-CNTs shells by using capillary action. Through adding PVP, the high-surface-tension GeO_2/NaCl solution could be induced into the inner hollow cavities of the PPy nanotubes to form a core–shell GeO_2/NaCl@PPy nanotubes composite. After further reducing GeO_2 to Ge and removing NaCl, the unique Ge@N-CNTs composite with Ge nanoparticles uniformly distributed in the N-CNTs could be obtained. The Ge@N-CNTs demonstrate enhanced cycling stability and excellent rate capability in comparison with Ge/N-CNTs, which could be attributed to the efficiently utilization of the void spaces provided by the uniformly distributed Ge nanoparticles. Moreover, the present strategy could be a general method to fabricate other 1D structured materials with enhanced electrochemical performance.

Experimental Section

Synthesis of PPy Nanotubes: PPy nanotubes were synthesized using a previously reported method.[50] In a typical synthesis process, methyl orange (0.25×10^{-3} M) was added in deionized water (100 mL), and then $FeCl_3$ (1.35 g) was dissolved to the solution. Then, the pyrrole monomer (5×10^{-3} M) was dissolved into the mixture dropwise. The solution was stirred for 24 h at room temperature. The thus-formed PPy nanotubes were washed with ethanol and deionized water several times. Then, PPy nanotubes with an inner cavity about 100 nm in diameter were obtained.

Synthesis of Ge@N-CNTs: PPy nanotubes (50 mg) were first added into deionized water (50 mL), followed by ultrasonication for 1.5 h to form a suspension. Meanwhile, GeO_2 (144 mg) were dissolved in NaOH solution (100 mL). After stirring for 1.5 h, the two solutions were mixed together, and then vigorously stirred for 20 min. The pH of the solution was slowly adjusted to 7 with dilute HCl. Then, PVP (MW = 10 000) (8 mg) was added into the solution. After drying out, the sample was annealed to 650 °C in a tube furnace at a rate of 5 °C min^{-1} in argon atmosphere. When the temperature reached 650 °C, the argon gas was replaced by H_2 gas,

and the reaction proceeds for 4 h. Finally, the sample was left to cool down to room temperature and then washed with ethanol and deionized water several times. To synthesize Ge/N-CNTs, the same method is used, but without adding PVP.

Materials Characterization: The crystalline structures of the samples were analyzed by powder XRD (GBC MMA) using Cu Kα radiation. Raman spectra were carried out by using JOBIN YVON HR800 Confocal system. Thermogravimetric analysis (TGA) tests were collected with a TGA instrument (Mettler-Toledo, Switzerland) from room temperature to 800 °C at a rate of 10 °C min^{-1} in air. The morphologies of the materials were investigated by scanning electron microscopy (JSM-7500FA, JEOL) and transmission electron microscopy (JEM-ARM200F, JEOL).

Electrochemical Measurement: 2032-type coin-cells were used to test the electrochemical performance. The electrodes were prepared by mixing the active material (80 wt%), Super P (10 wt%), and sodium carboxymethyl cellulose (10 wt%) in deionized water. The slurry was then cast on Cu foil and dried at 80 °C for 12 h in a vacuum oven. The working electrodes were prepared by punching the Cu film into discs 0.97 cm in diameter, and the loading mass of the active material for all the electrodes was at least 1.1 mg cm^{-2}. The coin-cells were assembled in an argon-filled glove box (Mbraun, Germany) with the prepared active material on Cu foil as working electrode, lithium foil as counter electrode, microporous polyethylene (Celgard 2400) as the separator, and 1 M $LiPF_6$ in a mixture of ethylene carbonate (EC), diethylcarbonate (DEC), and dimethyl carbonate (DMC) (3:4:4 by volume) as electrolyte. The assembly process was carried out in an argon-filled glove box with the oxygen and humidity levels under 0.1 ppm (Mbraun, Germany). The galvanostatically discharge and charge processes were carried out on a Land battery tester between 0.01 and 1.5 V versus Li^+/Li. Cyclic voltammetry was conducted with a Biologic VMP-3 electrochemical workstation.

Supporting Information

Supporting Information is available from the Wiley Online Library or from the author.

Acknowledgements

This research was financially supported by the Baosteel-Australia Joint Research and Development Centre (BA14006). The authors thank Dr. Tania Silver for critical reading of the manuscript, and acknowledge the use of the facilities in the University of Wollongong Electron Microscopy Center.

Conflict of Interest

The authors declare no conflict of interest.

[1] B. Dunn, H. Kamath, J. M. Tarascon, *Science* **2011**, *334*, 928.
[2] S. Xin, Z. Chang, X. Zhang, Y. Guo, *Natl. Sci. Rev.* **2016**, *4*, 1759.
[3] J. R. Dahn, T. Zheng, Y. Liu, J. S. Xue, *Science* **1995**, *270*, 590.
[4] W. Xiao, J. Zhou, L. Yu, D. Wang, X. W. Lou, *Angew. Chem. Int. Ed.* **2016**, *55*, 7427.
[5] T. Kennedy, M. Brandon, K. M. Ryan, *Adv. Mater.* **2016**, *28*, 5696.
[6] S. Wu, C. Han, J. Iocozzia, M. Lu, R. Ge, R. Xu, Z. Lin, *Angew. Chem. Int. Ed.* **2016**, *55*, 7898.
[7] K. H. Seng, M. H. Park, Z. P. Guo, H. K. Liu, J. Cho, *Nano Lett.* **2013**, *13*, 1230.
[8] K. H. Seng, M. H. Park, Z. P. Guo, H. K. Liu, J. Cho, *Angew. Chem. Int. Ed.* **2012**, *51*, 5657.
[9] G. Cui, L. Gu, N. Kaskhedikar, P. A. van Aken, J. Maier, *Electrochim. Acta* **2010**, *55*, 985.
[10] D. J. Xue, S. Xin, Y. Yan, K. C. Jiang, Y. X. Yin, Y. G. Guo, L. J. Wan, *J. Am. Chem. Soc.* **2012**, *134*, 2512.
[11] X. Liu, J. Hao, X. Liu, C. Chi, N. Li, F. Endres, Y. Zhang, Y. Li, J. Zhao, *Chem. Commun.* **2015**, *51*, 2064.
[12] W. Li, M. Li, Z. Yang, J. Xu, X. Zhong, J. Wang, L. Zeng, X. Liu, Y. Jiang, X. Wei, L. Gu, Y. Yu, *Small* **2015**, *11*, 2762.
[13] F. W. Yuan, H. J. Yang, H. Y. Tuan, *ACS Nano* **2012**, *6*, 9932.
[14] M. H. Park, Y. Cho, K. Kim, J. Kim, M. Liu, J. Cho, *Angew. Chem. Int. Ed.* **2011**, *50*, 9647.
[15] J. Liu, K. Song, C. Zhu, C. C. Chen, P. A. van Aken, J. Maier, Y. Yu, *ACS Nano* **2014**, *8*, 7051.
[16] Z. Chen, Y. Yan, S. Xin, W. Li, J. Qu, Y. G. Guo, W. G. Song, *J. Mater. Chem. A* **2013**, *1*, 11404.
[17] S. Xin, L. Yu, Y. You, H. P. Cong, Y. X. Yin, X. L. Du, Y. G. Guo, S. H. Yu, Y. Cui, J. B. Goodenough, *Nano Lett.* **2016**, *16*, 4560.
[18] Y. Sun, S. Jin, G. Yang, J. Wang, C. Wang, *ACS Nano* **2015**, *9*, 3479.
[19] W. J. Yu, C. Liu, P. X. Hou, L. Zhang, X. Y. Shan, F. Li, H. M. Cheng, *ACS Nano* **2015**, *9*, 5063.
[20] J. Q. Hu, X. M. Meng, Y. Jiang, C. S. Lee, S. T. Lee, *Adv. Mater.* **2003**, *15*, 70.
[21] A. Pandurangan, C. Morin, D. Qian, R. Andrews, M. Crocker, *Carbon* **2009**, *47*, 1708.
[22] G. A. Domrachev, A. M. Ob'edkov, B. S. Kaverin, A. A. Zaitsev, S. N. Titova, A. I. Kirillov, A. S. Strahkov, S. Y. Ketkov, E. G. Domracheva, K. B. Zhogova, *Chem. Vap. Deposition* **2006**, *12*, 357.
[23] Y. Yu, L. Gu, C. Wang, A. Dhanabalan, P. A. van Aken, J. Maier, *Angew. Chem. Int. Ed.* **2009**, *48*, 6485.
[24] X. Zhou, L. Yu, X. Y. Yu, X. W. D. Lou, *Adv. Energy Mater.* **2016**, *6*, 1601177.
[25] S. Xin, Y. G. Guo, L. J. Wan, *Acc. Chem. Res.* **2012**, *45*, 1759.
[26] B. Jiang, Y. He, B. Li, S. Zhao, S. Wang, Y. He, Z. Lin, *Angew. Chem. Int. Ed.* **2017**, *56*, 1869.
[27] B. Jiang, C. Han, B. Li, Y. He, Z. Lin, *ACS Nano* **2016**, *10*, 2728.
[28] S. Zhao, Z. Wang, Y. He, B. Jiang, Y. Harn, X. Liu, F. Yu, F. Feng, Q. Shen, Z. Lin, *ACS Energy Lett.* **2017**, *2*, 111.
[29] K. Huo, L. Wang, C. Peng, X. Peng, Y. Li, Q. Li, Z. Jin, P. K. Chu, *J. Mater. Chem. A* **2016**, *4*, 7585.
[30] C. Wu, Y. Jiang, P. Kopold, P. A. van Aken, J. Maier, Y. Yu, *Adv. Mater.* **2016**, *28*, 7276.
[31] C. Wu, P. Kopold, P. A. van Aken, J. Maier, Y. Yu, *Adv. Mater.* **2017**, *29*, 1604015.
[32] W. Li, Z. Yang, J. Cheng, X. Zhong, L. Gu, Y. Yu, *Nanoscale* **2014**, *6*, 4532.
[33] S. C. Tsang, Y. K. Chen, P. J. F. Harris, M. L. H. Green, *Nature* **1994**, *372*, 159.
[34] R. Kreizman, S. Y. Hong, J. Sloan, R. Popovitz-Biro, A. Albu-Yaron, G. Tobias, B. Ballesteros, B. G. Davis, M. L. Green, R. Tenne, *Angew. Chem. Int. Ed.* **2009**, *48*, 1230.
[35] G. Zheng, Q. Zhang, J. J. Cha, Y. Yang, W. Li, Z. W. Seh, Y. Cui, *Nano Lett.* **2013**, *13*, 1265.
[36] M. Haft, M. Grönke, M. Gellesch, S. Wurmehl, B. Büchner, M. Mertig, S. Hampel, *Carbon* **2016**, *101*, 352.
[37] Y. Zou, Y. Wang, *ACS Nano* **2011**, *5*, 8108.

[38] T. P. Kumar, R. Ramesh, Y. Y. Lin, G. T.-K. Fey, *Electrochem. Commun.* **2004**, *6*, 520.
[39] D. Ugarte, A. Chatelain, W. A. de Heer, *Science* **1996**, *274*, 1897.
[40] E. Dujardin, T. W. Ebbesen, H. Hiura, K. Tanigaki, *Science* **1994**, *265*, 1850.
[41] A. Mizev, A. Trofimenko, D. Schwabe, A. Viviani, *Eur. Phys. J.: Spec. Top.* **2013**, *219*, 89.
[42] E. Kim, Y. Xia, G. M. Whitesides, *J. Am. Chem. Soc.* **1996**, *118*, 5722.
[43] Y. Xiao, M. Cao, *Chem. Asian J.* **2014**, *9*, 2859.
[44] C. Zhong, J. Z. Wang, X. W. Gao, D. Wexler, H. K. Liu, *J. Mater. Chem. A* **2013**, *1*, 10798.
[45] S. Fang, L. F. Shen, H. Zheng, X. G. Zhang, *J. Mater. Chem. A* **2015**, *3*, 1498.
[46] Y. Xu, X. S. Zhu, X. S. Zhou, X. Liu, Y. X. Liu, Z. H. Dai, J. C. Bao, *J. Phys. Chem. C* **2014**, *118*, 28502.
[47] C. Yan, W. Xi, W. Si, J. Deng, O. G. Schmidt, *Adv. Mater.* **2013**, *25*, 539.
[48] T. Kennedy, E. Mullane, H. Geaney, M. Osiak, C. O'Dwyer, K. M. Ryan, *Nano Lett.* **2014**, *14*, 716.
[49] X. H. Liu, S. Huang, S. T. Picraux, J. Li, T. Zhu, J. Y. Huang, *Nano Lett.* **2011**, *11*, 3991.
[50] M. Li, W. Li, J. Liu, J. Yao, *J. Mater. Sci.: Mater. Electron.* **2013**, *24*, 906.

Received: March 21, 2017
Revised: April 7, 2017
Published online: May 30, 2017

